0273-2289/93/3940—0401$03.60

Acid Inhibition of Immobilized Cells

Quantitative Comparison of Model and Experiment

ROBERT KUHN, STEVEN PERETTI, AND DAVID OLLIS*

Chemical Engineering Department,
North Carolina State University, Raleigh, NC 27695

ABSTRACT

A quantitative comparision is offered between a kinetic model for product-inhibited, immobilized cell metabolism and a high-resolution scanning microfluorimetric characterization of variation of cell growth rates with position in immobilized cell cultures. The kinetic model is based exclusively on kinetic parameters derived from free cell suspension cultures and literature data for diffusion in biomass-loaded gels; the scanning microfluorimetry provides a high-resolution characterization of the point-by-point variation in cell growth rate in gel immobilized *E. coli* under cultivation with acid (formic, acetic) inhibition. The agreement between model and experiment is very good, indicating a strong potential for scanning microfluorimetry as a quantitative instrument in immobilized cell studies and for use of free cell kinetics in immobilized cell models.

Index Entries: Immobilized cells; acid inhibition; microfluorimetry.

INTRODUCTION

Numerous experimental and theoretical studies have firmly established the importance of mass-transfer influences on the behavior of immobilized cell systems. Mass-transfer influences typically restrict cell growth and activity to within 50–500 μm of the carrier surface for densely packed immobilized microbial systems (*1–5*). Mass-transfer restrictions can thus severely limit the productivity of immobilized cell reactors.

*Author to whom all correspondence and reprint requests should be addressed.

Many studies have focused on restrictions on the delivery of rate-influencing substrates, such as oxygen or the carbon source. Recently, several researchers have also recognized the importance of mass-transfer restrictions on the removal of inhibitory products (*6–8*).

Mass-transport influences on the delivery and removal rates of compounds that influence pH can lead to gradients in pH within the immobilized-cell phase. Changes in pH have been measured across nitrifying (*9*) and denitrifying (*10*) biofilms, and within cultures of agar-entrapped yeast (*11*) and immobilized *E. coli* (*12*). Both radiolabeling pulse-chase (*12*) and ^{32}P-NMR techniques (*13*) have demonstrated that weak acid inhibition can exist in immobilized cell environments, even when the bulk solution is free of substantial acid. Weak acid inhibition of immobilized *Lactobacillus delbrueckii* was recently explored, including a model accounting for diffusional restrictions on proton and lactate removal, and the consequent effect on local growth and metabolic rates. Transport of product lactic acid was considered to be the primary avenue for proton transport (*14*).

Buffers are often added to a medium; these pH stabilizers can also greatly enhance the net proton transport rate in a pH gradient via a carrier-mediated facilitated diffusion mechanism. Because of the relatively low concentration of free protons, a small level of buffer-facilitated transport will easily surpass free proton diffusion as the dominant transport mode (*15*); this influence has been modeled in immobilized enzyme systems (*16–18*).

The present study combines full modeling of weak acid and buffer transport with detailed consideration of the metabolic reactions associated with living cells and weak acid product inhibition of cell growth. The intrinsic microbial kinetics were developed from free cell kinetics of batch, suspension culture. Details are provided in references (*19,20*). The simplified form of the free cell model was found to describe batch growth quite well; this model is summarized in Table 1. The equations for specific growth rate, μ, and for specific substrate consumption rate, q_s, include the following important features:

1. Monod dependence on carbon substrate;
2. Mild inhibition by protons (second term in square brackets);
3. Inhibition by neutral form of formic and acetic acid products; and
4. Existence of separate thresholds at which μ and q_s became zero.

The parameter values for this model were derived from free cell initial and time-varying rate data for batch cultures, the literature, and yield experiments; these values are summarized in Table 2 (*20*).

A corresponding reaction and diffusion immobilized cell model for cell metabolism in buffered media was developed, and is summarized in Table 3. The key assumptions in deriving this model were the following (*19,20*):

Table 1
Batch Culture Model: Free Cells (*20*)

Cell mass: $(dC_x / dt) = \mu C_x$

Substrate (glucose): $(dC_s / dt) = - q_S C_x$

Buffer ($MOPS^-$): $(dC_{B^-} / dt) = - Y_{H^+/S} q_s C_x$

Acetate: $(dC_{Ac} / dt) = q_{Ac} = Y_{Ac/S} q_S C_x$

Formate $(dC_F / dt) = - q_F C_x = Y_{F/S} q_S C_x$

Where:

$$\mu = \mu_{max} [(C_S / K_S + C_S)] [(K_I^{H^+} / K_I^{H^+} + C_{H^+})]$$
$$[(K_{I1g}^{AcH} / K_{I1g}^{AcH} + C_{AcH}) - K_{I2g}^{AcH} C_{AcH}]$$
$$[(K_{I1g}^{FH} / K_{I1g}^{FH} + C_{FH}) - K_{I2g}^{FH} C_{AcH}]$$

$$q_S = (\mu_{max} / Y_{X/S}) [(C_S / K_S + C_S)] [(K_I^{H^+} / K_I^{H^+} + C_{H^+})]$$
$$[(K_{I1m}^{AcH} / K_{I1m}^{AcH} + C_{AcH}) - K_{I2m}^{AcH} C_{AcH}]$$
$$[(K_{I1m}^{FH} / K_{I1m}^{FH} + C_{FH}) - K_{I2m}^{FH} C_{FH}]$$

$$C_{FH} = (C_H + C_F / C_{H^+} + K_a^F) C_{AcH} = (C_H + C_{Ac} / C_{H^+} + K_a^{Ac})$$
$$C_{H^+} = K_a^{BH} (C_B - C_{B^-} / C_{B^-})$$

1. Free cell kinetics apply at every point within the immobilization matrix;
2. A pseudo-steady state applies, since the time scale for cell growth is much longer than the time scale for development of pseudo-steady diffusion profiles;
3. Diffusivities of the weak acid salts are given by those of the individual weak acid conjugates, and the dissociated and undissociated forms have equal diffusivities;
4. Influence of charge of anionic matrix alginate is negligible (low charge concentration, large pores, relatively high medium ionic strength);
5. Buffer species are at equilibrium locally within the matrix;
6. Proton diffusion is overwhelmingly the result of facilitated transport by protonated buffer;
7. The weak acids are predominantly present in dissociated form; and
8. Glucose is the only limiting substrate.

The calculational approach for solution of these equations was as follows: In dimensionless form, the equations of Table 3 were solved using a multiple-shooting technique (DVBPMS) available on IMSL. The solution procedure involved first solving for the critical radius value within

Table 2
Parameters Values for Free Cell Model (*20*)

Parameter	Value	Source*
K_S	65 μM	(*21*)
$K_I^{H^+}$	6.14 μM	i
K_{Ig1}^{AcH}	0.827 mM	i
K_{Ig2}^{AcH}	0.0312 mM^{-1}	i
K_{Ig1}^{FH}	0.079 mM	i
K_{Ig2}^{FH}	1.56 mM^{-1}	i
K_{Im1}^{AcH}	2.81 mM	b
K_{Im2}^{AcH}	0.000493 mM^{-1}	b
K_{Im1}^{FH}	0.132 mM	b
K_{Im2}^{fH}	0.031 mM^{-1}	b
pK_a^{AcH}	4.756	(*22*)
pK_a^{FH}	3.756	(*22*)
pK_a^{MOPS}	6.98	(*22*)
μ_{max}	0.481 h^{-1}	i
$Y_{X/S}$	18.9 g/mol	b
$Y_{H^+/S}$	2.52 mol/mol	b
$Y_{Ac/S}$	0.72 mol/mol	b
$Y_{F/S}$	1.51 mol/mol	b
$Y_{X/OD}$	0.54 g cells/U OD (600nm)	e

b: Batch culture data.
e: Experimentally determined.
i: Initial rate data.

the immobilized gel spherical bead at which the substrate flux became zero. If $q_s > 0$ at $r = 0$, $r_{crit} = 0$. Otherwise, r_{crit} corresponded to the point where q_s became zero owing to substrate exhaustion, proton inhibition, and/or weak acid inhibition. An iterative search routine was implemented to locate r_{crit} within a desired tolerance $[0 < q_s(r_{crit}) < 0.01]$.

MATERIALS AND METHODS (*19*)

Strain and Culture Conditions

The *E. coli* strain employed, BK25, contained a formate dehydrogenase mutation that disables the formate hydrogen-lyase pathway, thus avoiding decomposition of formate into carbon dioxide and hydrogen. Two other mutations (*thyA* and *deoB*) allow efficient DNA labeling with bromi-

Table 3
Simplified Immobilized Cell Model (*20*)

Substrate (S): $(1/r^2)(d/dr)[r^2 D_S^{eff}(dC_s/dr)] = q_S C_x$

Unprotonated buffer (B^-): $(1/r^2)(d/dr)[r^2 D_B^{eff}(dC_{B^-}/dr)] = Y_{H^+/S}\, q_S C_x$

Acetic acid (Ac): $(1/r^2)(d/dr)[r^2 D_{Ac}^{eff}(dC_{AcH}/dr)] +$

$(1/r^2)(d/dr)[r^2 D_{Ac}^{eff}(dC_{Ac^-}/dr)] = -Y_{Ac/S}\, q_S C_x$

Formic acid (F): $(1/r^2)(d/dr)[r^2 D_F^{eff}(dC_{FH}/dr)] +$

$(1/r^2)(d/dr)[r^2 D_F^{eff}(dC_{F^-}/dr)] = -Y_{F/S}\, q_S C_x$

Where: $D_i^{eff} = D_i^{Gel}[1 - (C_x/C_X^{max}) + D_i^x (C_x/C_X^{max})$

$$\mu = \mu_{max}[(C_S/K_S + C_S)][(K_I^{H^+}/K_I^{H^+} + C_{H^+})]$$
$$[(K_{I1g}^{AcH}/K_{I1g}^{AcH} + C_{AcH}) - K_{I2g}^{AcH} C_{AcH}]$$
$$[(K_{I1g}^{FH}/K_{I1g}^{FH} + C_{FH}) - K_{I2g}^{FH} C_{AcH}]$$

$$q_S = (\mu_{max}/Y_{X/S})[(C_S/K_S + C_S)][(K_I^{H^+}/K_I^{H^+} + C_{H^+})]$$
$$[(K_{I1m}^{AcH}/K_{I1m}^{AcH} + C_{AcH}) - K_{I2m}^{AcH} C_{AcH}]$$
$$[(K_{I1m}^{FH}/K_{I1m}^{FH} + C_{FH}) - K_{I2m}^{FH} C_{FH}]$$

$$C_{H^+} = K_a^{BH}(C_B^o - C_{B^-}/C_B)\, C_{FH} = (C_H + C_F/C_{H^+} \$ K_a^{FH})$$

$C_{AcH} = (C_H + C_{Ac}/C_{H^+} + K_a^{AcH})\, C_B^o = C_{BH} + C_{B^-}$, $C_{Ac} = C_{AcH} + C_{Ac^-}$, $C_F = C_{FH} + C_{F^-}$

Boundary Conditions: at $r = r_{crit}$; $(dC_i/dr) = 0$, at $r = r_o$; C_i^o

uracil for total DNA measurements. All experiments were conducted at 37°C in MOPS-buffered MM5 minimal medium (*21*). Anaerobic conditions were maintained by sparging with 1% CO_2/99% N_2 gas.

Immobilization and DNA Labeling

Immobilized cell studies were conducted to test model predictions. Spatial variation in DNA synthesis rates within the beads were determined as a function of bulk environmental conditions using bromouracil (BrU) pulse-labeling (*23*). Four liters of anaerobically grown, midlog-phase cells were spun down (10K RPM, 10 min), resuspended in 150 m*M* NaCl, and mixed with Na-alginate (Protanol LF 20.60) to give a final concentration 2.5% (w/v) alginate. Beads were first formed by allowing discrete drops of cell/alginate suspension to fall from an 18-gage syringe into a solution of 100 m*M* $SrCl_2$/10 m*M* MOPS/100 μM thymine (pH=7.0),

and were then allowed to gel for 2 h. The bead preparation procedure resulted in the formation of gel beads averaging 3.06 mm diameter with a measured uniform cell loading of 28.6 g cells/L of bead volume. Cell loading and bead size were determined as described previously (*23*). After gelation, the beads were used immediately in DNA pulse-labeling experiments to test the effect of bulk environmental conditions (glucose concentration, pH, and MOPS buffer concentration) on the radial growth rate profiles. Pulse-labeling with BrU under anaerobic conditions was conducted essentially as described previously (*23*), except that Bellco spinner jars with a 500-mL working volume were used as the labeling flasks.

Analysis of Spatial Variations in DNA Synthesis Rate

The bead samples were prepared and stained for BrU incorporation (DNA synthesis) as described previously (*23*), except for 2% EDC in 50 m*M* PIPES (pH 7.0).

RESULTS

Model Simulations

General Trends

The base-case parameters for the model simulations are shown in Table 4. The bulk concentrations simulate typical operating conditions, and all other parameters were derived from independent experiments or the literature. The cell loading used was 90% of the maximum, simulating a densely packed carrier. Any parameter changes are noted in the figure legends.

Typical trends calculated within the biocatalyst support are shown in Fig. 1. Mass-transfer influences lead to a decline in glucose and buffer ion concentrations with distance inward from the bead surface, with an opposing gradient in undissociated buffer molecules (not shown). Buffer ion depletion leads to a steep pH gradient within the bead. Diffusional limitations also lead to a buildup of acetate and formate within the immobilized cell phase. In combination with the pH drop, this results in the accumulation of high levels of the inhibitory, undissociated forms of weak acid products, which may ultimately halt cell growth and slow metabolism deep within the carrier.

At high bulk glucose levels, glucose is always in excess and does not influence the kinetics. Under these acid-inhibited conditions, the specific growth rate declines more rapidly with position from the bead surface than does the specific glucose consumption rate, as the weak acid buildup inhibits growth more strongly than substrate consumption. This effect leads to a decline in the overall cell yield for the immobilized cells, as has been observed experimentally by others (*12,24*).

Table 4
Parameters Used in Simulations

Parameter	Value	Source*
C_S^o	50 mM**	A
C_B^o	80 mM**	A
C_{Ac}^o	0 mM**	A
C_F^o	0 mM**	A
C_X	270 g/L**	A
C_X^{max}	300 g/L	(*21*)
pH^o	7.0**	A
D_i^{gel}	$0.9 \times D_i^o$	(*25*)
D_i^X	$0.2 \times D_i^o$	(*26*)
D_{Ac}^o	1.66×10^{-5}cm²/s	C
D_F^o	1.83×10^{-5}cm²/s	C
D_B^o	9.16×10^{-6}cm²/s	D
D_S^o	9.25×10^{-6}cm²/s	D
pK_a^{AcH}	4.76	(*27*)
pK_a^{FH}	3.76	(*27*)
pK_a^{BH}	6.98**	(*27*)
K_S	65 μM	(*21*)
K_I^{H+}	6.14 μM	B
K_{Ig1}^{AcH}	0.827 mM	B
K_{Ig2}^{AcH}	0.0312 mM^{-1}	B
K_{Ig1}^{FH}	0.079 mM	B
K_{Ig2}^{FH}	1.56 mM^{-1}	B
K_{Im1}^{AcH}	2.81 mM	B
K_{Im2}^{AcH}	0.000493 mM^{-1}	B
K_{Im1}^{FH}	0.132 mM	B
K_{Im2}^{fH}	0.031 mM^{-1}	B
μ_{max}	0.481 h^{-1}	B
$Y_{X/S}$	18.9 g/mol	B
$Y_{H^+/S}$	2.52 mol/mol	B
$Y_{Ac/S}$	0.72 mol/mol	B
$Y_{F/S}$	1.51 mol/mol	B
r_o	500 μm**	A

Parameters were varied during the simulations and values shown represent the base case. † A, simulation base-case or experimental conditions; B, experimentally determined; C, diffusivities in water at 25°C obtained from Perry and Chilton, diffusivity at 37°C estimated by assuming Dv/T=constant. D, diffusivity in water at 37°C estimated by the Wilke-Chang correlation.

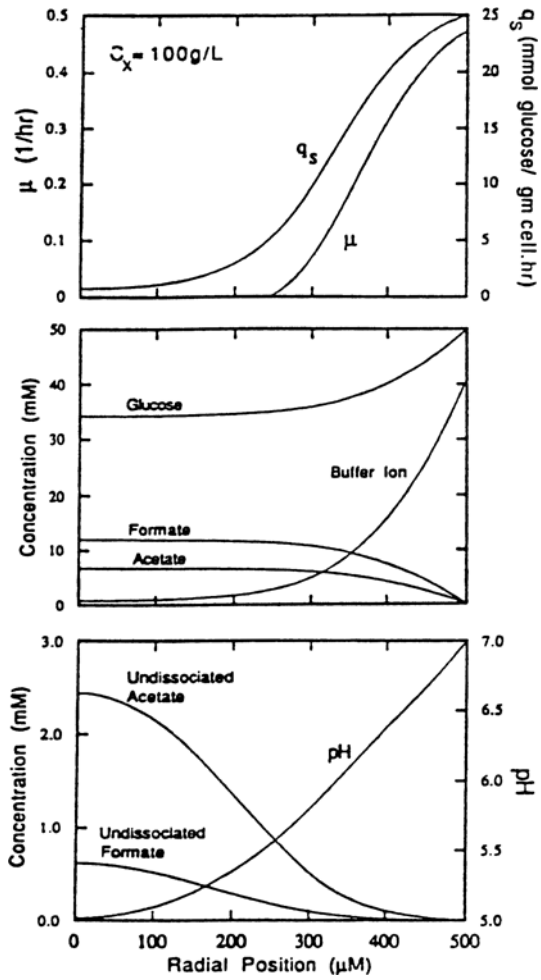

Fig. 1. Calculated profiles: (Top) specific substrate rate, q_s, and specific growth rate, μ (Center) substrate glucose, product formate and acetate, and buffer ion B^-. (Bottom) pH and inhibitory, undissociated forms of acetic and formic acids. ([20] Reprinted by permission of ACS and AIChE.)

Experimental Analysis

A simple experiment was conducted to test the general validity of the modeling approach. Newly formed beads with a moderate, uniform cell loading were exposed for 40 min to different bulk solution conditions (variable bulk buffer, proton, and glucose concentrations) and were simultaneously pulse-labeled for active DNA synthesis with the thymine analog BrU. Thin center bead cross-sections were prepared and fluorescently stained for incorporated BrU (DNA synthesis). Under balanced growth conditions, specific DNA synthesis rate is proportional to specific growth rate. The base case conditions for the experiment are shown in Table 5.

Changes in parameter values are noted in the figure legends.

Table 5
Base Case Conditions
for Pulse-Labeling Experiment

C_X = 28.6 g dcw/L	C_B^o = 80 m*M*
r_S = 1530 μm	C_S^o = 50 m*M*
pH^o = 7.0	C_{AC}^o = 0 m*M*
$pK_a^{buffer}(MOPS)$ = 6.98	C_F^o = 0 m*M*

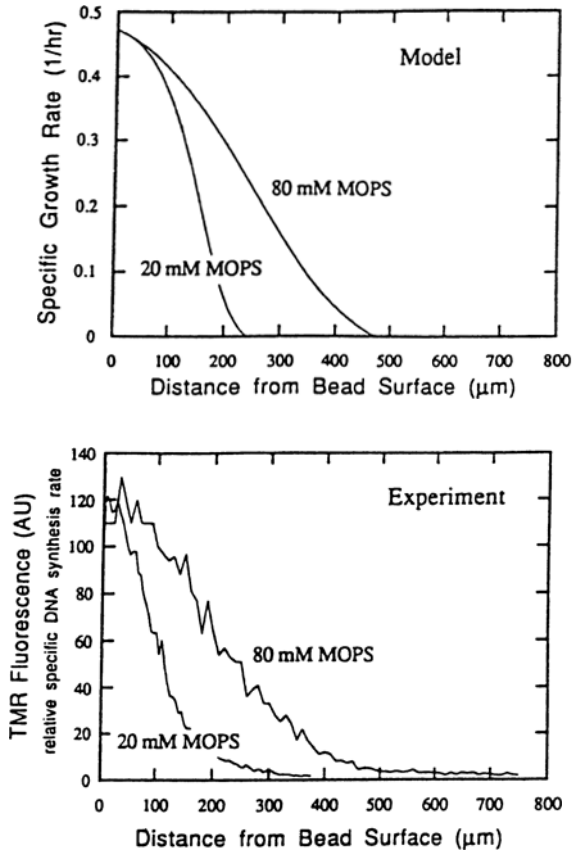

Fig. 2. Comparison of (top) *a priori* model predictions of growth rate distributions to (bottom) experimentally measured spatial profiles of specific DNA synthesis rates for samples exposed to different bulk buffer levels. ([20] Reprinted by permission of ACS and AIChE.)

The effect of bulk buffer concentration on radial growth rate profiles, predicted and experimental, is shown in Fig. 2. Lowering the bulk buffer level decreases the efficiency of proton removal from the immobilized cell phase, leading to a sharp drop in pH with an attendant increase in proton and weak acid inhibition effects and a thinning of the region of active cell growth. The experimental results mirror the model predictions quite well.

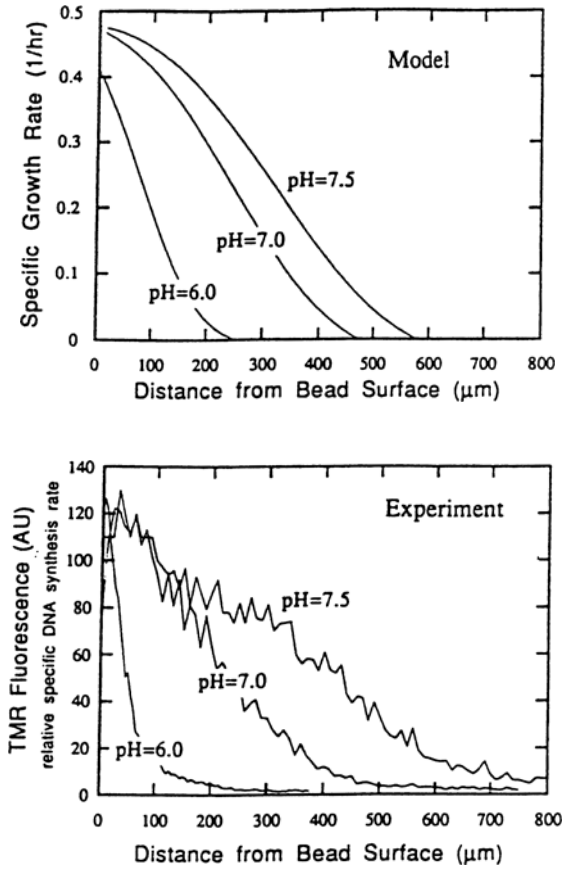

Fig. 3. Comparison of (top) *a priori* model predictions of growth rate distributions to (bottom) experimentally measured spatial profiles of specific DNA synthesis rates for samples exposed to different bulk pHs. ([*20*] Reprinted by permission of ACS and AIChE.)

We emphasize that the parameters were obtained *a priori* from free (suspension) cell data of our own or the literature: No adjustable parameters remained. The general agreement of the model and experiment also supports our central assumption, namely that a strong correlation exists between the actual specific growth rate and the measured specific DNA synthesis rate.

Figure 3 compares the predicted growth rate profiles with experimentally determined DNA synthesis rate profiles exhibited at different bulk pHs. Increasing the bulk pH in the range shown here increases the efficiency of proton removal from the immobilized cell phase and shifts the weak acid species equilibrium distribution away from the inhibitory undissociated form. The net result is an increase the depth of cell growth. The correct experimental trends are predicted, with a slight underestimate of growth rate profile at the most basic pH (7.5).

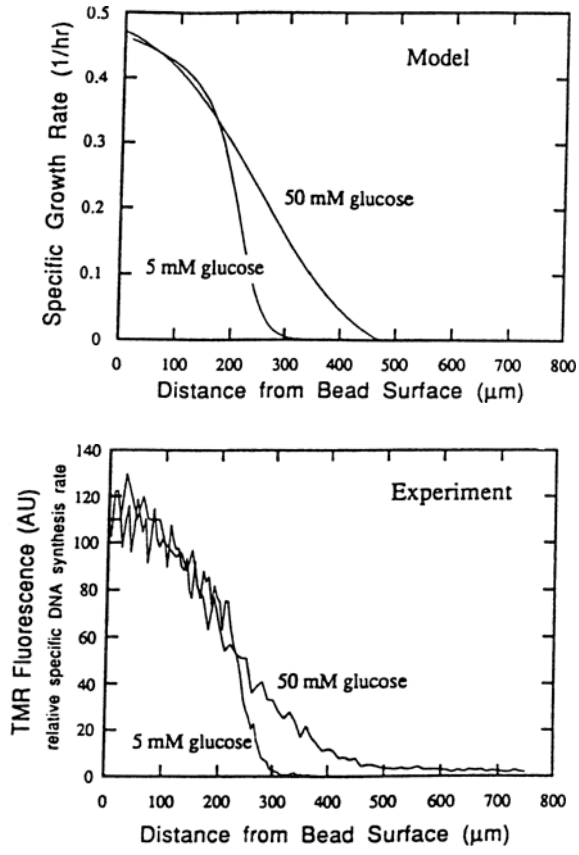

Fig. 4. Comparison of (top) *a priori* model predictions of growth rate distributions to (bottom) experimentally measured spatial profiles of specific DNA synthesis rates for samples exposed to different bulk glucose levels. ([*20*] Reprinted by permission of ACS and AIChE.)

The influence of bulk glucose level is demonstrated and predicted in Fig. 4 for 5- and 50-m*M* bulk glucose levels. The analysis compares quite favorably again to the experimental results. At the low bulk glucose level, the inner boundary of the actively growing cell layer is determined primarily by glucose exhaustion, not product inhibition. Since *E. coli* has a high affinity for glucose ($K_s < 0.1$ m*M*), there is a relatively sharp drop in growth rate because the kinetics are affected only at very low glucose levels (below 0.5 m*M*). As indicated in separate calculations (*19,20*), the model predicts that above 5 m*M* glucose, the system becomes increasingly influenced by acid inhibition effects, and above 20 m*M* bulk glucose, the system is under complete acid-inhibition control. This predicted inhibition behavior is consistent with the experimental data of Fig. 4, which show that a 10-fold increase in limiting substrate concentration results in an only somewhat greater depth of cell growth.

In experiments reported elsewhere (*20*), we have shown that volume-averaged, recombinant protein production by anaerobically grown, immobilized, recombinant *E. coli* suffered similar limitations by acid inhibition. Net recombinant protein production was shown to decrease with decreasing bulk buffer levels. This result indicated that weak acid inhibition can directly limit productivity as well as active cell growth in immobilized cell systems.

CONCLUSIONS

A mechanistically detailed model of an anaerobic immobilized cell system that produces inhibitory weak acid products has been developed. The model accounts for the transport, metabolic reaction, and ionization equilibrium (where appropriate) of the carbon source, the main buffer, protons, and two inhibitory weak acid products. The immobilized cell model incorporates no adjustable parameters, and uses only physical constants derived from the literature and from free cell kinetic studies. For the first time, the ability of an immobilized cell model to predict growth rate profiles within an immobilization support was directly tested experimentally under different bulk environmental conditions. These results confirm that the model was able to predict changes in growth rate profiles correctly with variation in each of three important operating variables: limiting concentration of bulk substrate, bulk buffer level, and bulk pH. This study indicates that immobilized cell systems can be effectively modeled through careful consideration of the dominant physical processes and that gel-immobilized *E. coli* cells exhibit behavior similar to free cells.

The behavior of the present immobilized cell system depends on the bulk levels of substrate, weak acids, buffer and protons (pH), buffer pK_a, cell loading, carrier dimensions, and both the diffusional and intrinsic reaction kinetics. Realistic immobilized cell models are essential in understanding these complex interactions. Anaerobic, alginate-entrapped *E. coli* cells exhibit strong mass-transfer resistance to buffer transport (proton removal via facilitated transport), weak acid removal, and substrate delivery. These mass-transfer effects were shown to influence the overall active cell loading and growth rate, biomass yield, and productivity strongly. Since acid production and weak acid inhibition are quite common phenomena, these observed effects may be widespread, but generally unrecognized for systems as diverse as waste water treatment biofilms and immobilized mammalian cells. The general modeling approach described here is broadly applicable if proper consideration is given to the dissociation equilibrium regimes of the important rate- and pH-influencing species. A procedure for identifying the important metabolic reactions that influence both pH and the primary buffering species is provided elsewhere (*20*).

ACKNOWLEDGMENT

This work was supported by the National Science Foundation under grant BCS No. 98915680.

REFERENCES

1. Baudet, C., Barbotin, J. M., and Guespin-Michel, J. (1983), *Appl. Environ. Microbiol.* **45,** 297.
2. Eikmeier, H., Westimeier, F., and Rehm, H. J. (1984), *Appl. Microbiol. Biotechnol.* **19,** 53.
3. Monbouquette, H. G., Sayles, G. D., and Ollis, D. F. (1990), *Biotechnol. Bioeng.* **35,** 609.
4. Nasri, M., Sayadi, S., Barbotin, J. N., and Thomas, D. (1987), *J. Biotechnol.* **6,** 147.
5. Shinmyo, A., Kimura, H., and Okada, H. (1982), *Eur. J. Appl. Microbiol. Biotechnol.* **14,** 7.
6. Sayles, G. D. and Ollis, D. F. (1990), *Biotechnol. Progress.* **6,** 153.
7. Luong, J. H. T. (1985), *Biotechnol. Bioeng.* **27,** 1652.
8. Monbouquette, H. G., Sayles, G. D., and Ollis, D. F. (1990), *Biotechnol. Bioeng.* **35,** 609.
9. Szwerinski, H., Arvin, E., and Harremoes, P. (1986), *Water Res.* **20,** 971.
10. Arvin, E. and Kristensen, G. H. (1982), *Water Sci. Tech.* **14,** 833.
11. Kim, J. Y. and Lee, Y. H. (1989), *Biotechnol. Bioeng.* **34,** 131.
12. Stewart, P. S. and Robertson, C. R. (1988), *Appl. Environ. Microbiol.* **54,** 2464.
13. Briasco, C. A., Karel, S. F., and Robertson, C. R. (1990), *Biotechnol. Bioeng.* **36,** 887.
14. Yabannavar, V. M. and Wang, D. I. C. (1991), *Biotechnol. Bioeng.* **37,** 544.
15. Engasser, J. M. and Wilhelm-Despres, A. M. (1980), *Chem. Eng. Sci.* **35,** 669.
16. Engasser, J. M. and Horvath, C. (1974), *Biochem. Biophys. Acta* **358,** 178.
17. Ruckenstein, E. and Rajora, P. (1985), *Biotechnol. Bioeng.* **27,** 807.
18. Rukenstein, E. and Sasidhar, V. (1984), *Chem. Eng. Sci.* **39,** 1185.
19. Kuhn, R., Peretti, S., and Ollis, D. F. (1992), *Biotechnol. Bioeng.* (submitted).
20. Kuhn, R. (1991), PhD. thesis, NCSU.
21. Reiling, H. E., Laurila, H., and Fiecher, A. (1985), *J. Biotechnol.* **2,** 191.
22. Perrin, D. D. and Dempsey, B. (1974), *Buffers for pH and Metal Ion Control,* Chapman and Hall, London.
23. Kuhn, R. H., Peretti, S. W., and Ollis, D. F. (1991), *Biotechnol. Bioeng.* **38,** 340.
24. Karel, S. J. and Robertson, C. R. (1989), *Biotechnol. Bioeng.* **34,** 337.
25. Axelsson, A. and Persson, B. (1988), 231.
26. Scott, C. D., Woodward, C. A., and Thompson, J. E. (1989), *Enzyme Microb. Technol.* **11,** 258.
27. Perrin, D. D. and Dempsey, B. (1974), *Buffers for pH and Metal Ion Control,* Chapman and Hall, London.